CrossMark

ORIGINAL ARTICLE

Existence Conditions and Formation Process of Second Type of Spiral Loop Particle Accumulation Structure (SL-2 PAS) in Half-zone Liquid Bridge

A. Toyama[1] · M. Gotoda[1] · T. Kaneko[1] · I. Ueno[1]

© Springer Science+Business Media Dordrecht 2017

Abstract We focus on unique phenomena known as particle accumulation structure (PAS), especially on the conditions of the existence for second-type spiral loop PAS (SL-2 PAS) and on their formation processes under normal gravity. We investigate the existence conditions as functions the aspect ratio of the liquid bridge and the Marangoni number, the intensity of the thermocapillary effect. We discuss the differences among SL-1 PAS, SL-2 PAS and the flow field without PAS through observation of the solid-like structures of the PAS in a rotating frame of reference with the hydrothermal wave, and through monitoring of the surface temperature by infrared camera. We evaluate the formation time of PAS by employing a modified accumulation measure by considering the effect of the particles' size.

✉ I. Ueno
ich@rs.tus.ac.jp

A. Toyama
7511085@alumni.tus.ac.jp

1   Department of Mechanical Engineering, Faculty of Science
    & Technology, Tokyo University of Science, 2641 Yamazaki,
    Noda, Chiba 278–8510, Japan

Introduction

A difference in surface tension over a free surface due to a difference in temperature realizes a convective motion of a fluid if the temperature coefficient of surface tension is not zero. Such an induced flow is generally called thermocapillary-driven convection by the thermocapillary effect. This effect becomes more significant under microgravity and microscale conditions, where the buoyancy effect can be almost excluded. There have been a number of studies on the induced convection in a half-zone (HZ) liquid bridge, which is suitable for the study of the thermocapillary effect. In the HZ liquid bridge, where the liquid is held between two cylindrical coaxial rods, with the top rod heated and the bottom rod cooled, the convection emerges as a result of the thermocapillary effect over the free surface. The intensity of the thermocapillary flow is generally described by the non-dimensional Marangoni number, defined as

$$\mathrm{Ma} = \frac{|\sigma_T| \, \Delta T \, H}{\rho \nu \kappa} = \mathrm{Re} \cdot \mathrm{Pr},$$

where σ_T is the temperature coefficient of the surface tension σ of the fluid; $\Delta T (= T_\mathrm{H} - T_\mathrm{C})$ is the temperature difference between the top rod at T_H and the bottom rod at T_C; H is the height of the liquid bridge; ρ, ν, and κ are the density, kinematic viscosity, and thermal diffusivity of the fluid, respectively. The Marangoni number is described as the product of the thermocapillary Reynolds number Re and the Prandtl number Pr $(= \nu/\kappa)$.

It has been known that a three-dimensional time-dependent flow ('oscillatory flow') occurs from a two-dimensional time-independent flow ('steady flow') when the temperature difference exceeds the threshold in the case of high Prandtl number fluid (Wanschura et al. 1995). The oscillatory flow has a modal structure in azimuthal direction, whose azimuthal modal number is described here by m. The flow fields are generally visualized by adding tiny particles as the tracers in the experiments, and the oscillatory flows can be categorized into regimes by the patterns of the particles suspended in the bridge observed through the top rod (e.g., Hirata et al. 1997; Ueno et al. 2003). Figure 1 illustrates typical examples of the top views of the flow patterns as a function of the temperature difference. Each image indicates the path lines by integrating frames (as conducted by Kuhlmann et al. (2014) and Gotoda et al. (2015)). Frame (a) indicates the steady flow (integrated for 5 second), in which the particles move only in the r-z plane; one cannot detect any azimuthal motion of the particles. And there exists a 'particle-free zone' in the interior region near the center of the bridge (Ueno et al. 2003), where the particles never penetrate in the flow. This region is also called 'depletion zone' (Kuhlmann et al. 2014). As increasing the temperature difference, the flow exhibits a transition to the oscillatory flows (frame (b) and (c) drawn in the rotating frame of reference with the hydrothermal wave (integrated for 5 second)), and the particles form morphological structures with an azimuthal mode number ($m = 3$ in this case). Under the smaller temperature difference above the threshold, the particles still travel in outer region of the liquid bridge but disperse in the azimuthal direction. The depletion zone exhibits a triangle shape under this condition. Under the larger temperature difference, on the other hand, particles segregate such that their distribution becomes inhomogeneous and, eventually, time-independent in the mean. This unique phenomenon is called the 'particle accumulation structure (PAS)', which was named by Schwabe et al. (1996) and Tanaka et al. (2006) successfully

reproduced the PAS, and firstly indicated two fundamental shapes, which they named the SL-1 PAS and SL-2 PAS depending on the structure by the particles accumulation (Fig. 2).

Much has been known about the SL-1 PAS because it has been the main subject of previous studies. These studies undertook experiments to examine the conditions under which the SL-1 PAS is formed as functions of the Marangoni number, the liquid-bridge aspect ratio (Tanaka et al. 2006; Schwabe et al. 2007; Gotoda et al. 2015), the volume ratio (Abe et al. 2007; Melnikov et al. 2014; Watanabe et al. 2014), and the different particle sizes (Schwabe et al. 2006, 2007; Gotoda et al. 2015. The formation time of the PAS has also been focused by several groups (Schwabe et al. 2007; Kuhlmann and Muldoon 2012; Gotoda et al. 2015)

Focusing on the main mechanism of PAS formation, two models have been proposed by different groups. Pushkin et al. (2011) proposed 'phase locking' considering the effect of inertia and the 'synchronization' of finite-size particles and the flow field by hydrothermal wave instability. It was suggested that the presence of a phase-locking region with respect to the frequency of the particle turnover motion and the wave oscillation frequency (Melnikov et al. 2013). On the other hand, Hofmann and Kuhlmann (2011) proposed the 'particle free–surface interaction (PSI)' model, which assumed that the PAS is caused by particle-boundary interaction. Their group focused on that interaction length and investigated the various shapes of the PAS (strange PAS, tubular PAS, line-like PAS and period-doubled PAS) under the effects of thermocapillary Reynolds number and Stokes number (corresponding to the size of particles) by numerical simulations (Mukin and Kuhlmann 2013; Muldoon and Kuhlmann 2014). Further they employed an analytical model that the flow was a semi-quantitative approximation of the hydrothermal waves and evaluated the formation of PAS quantitatively (Kuhlmann and Muldoon 2012; Muldoon and Kuhlmann 2013). Muldoon and Kuhlmann (2016) clarified the relative importance of inertia and particle–surface interaction for Pr = 4.

Fig. 1 Typical example of flow fields as viewed from above when $\Gamma = 0.68$ and (**a**) Ma = 1.3×10^4 (for 5 s), (**b**) Ma = 2.7×10^4 (for 5 s), and (**c**) Ma = 3.0×10^4 (for 5 s). Noted that the frames (**b**) and (**c**) indicate the image obtained in the rotating frame of reference regarding to the hydrothermal wave. The rotating direction of the hydrothermal wave in frames (**b**) and (**c**) is counterclockwise

1 mm

Rod periphery

(a)   (b)   (c)

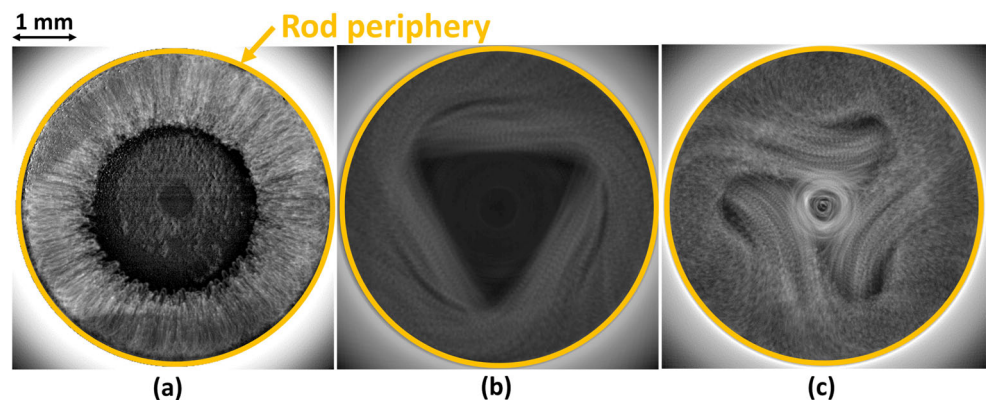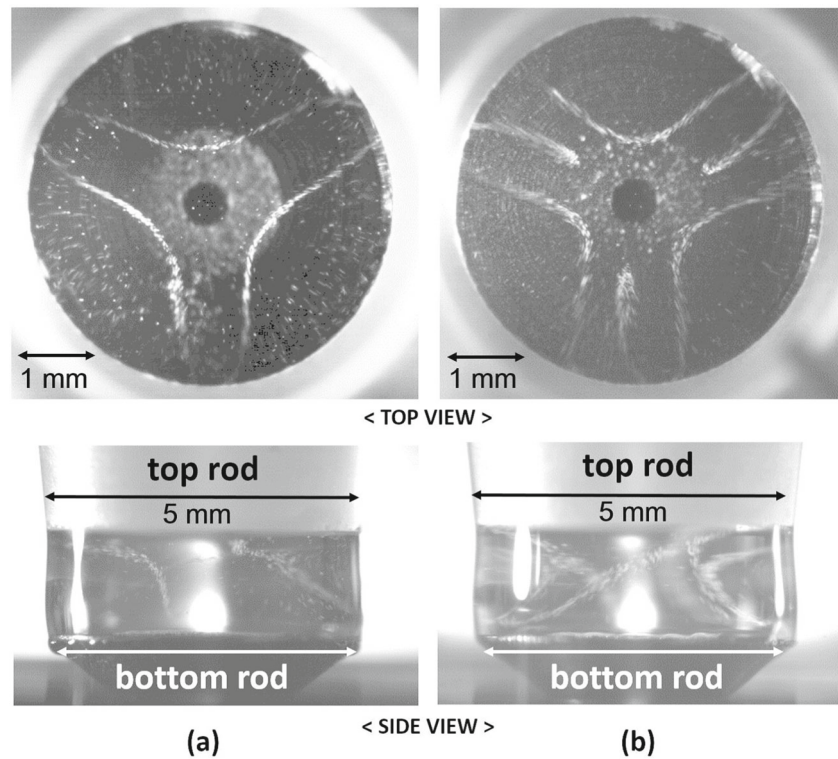**Fig. 2** Snapshots of particle accumulation as viewed from above (top row) and from the side (bottom row) for (**a**) SL-1 PAS when Ma = 4.7×10^4 and (**b**) SL-2 PAS when Ma = 5.8×10^4. The direction of the hydrothermal wave is counterclockwise for both cases in the top row, and is from right to left in the bottom row

Although there have been many studies of the PAS, the SL-2 PAS has not been examined as much as the SL-1 PAS because its structure is more complicated and therefore does not arise so easily. Tanaka et al. (2006) determined the conditions under which the PAS arised by changing the aspect ratio of the liquid bridge and also the temperature difference. They conducted a series of experiments under conditions of the ambient temperature at about −20 °C in order to realize a large temperature difference while suppressing the evaporation of the fluid. Schwabe et al. (2007) identified the SL-2 PAS of $m = 2$, by using n-decane (Pr = 15) as the test fluid. Niigaki and Ueno (2012) evaluated the velocities of particles forming the SL-2 PAS of $m = 3$ by applying three-dimensional particle tracking velocimetry (3D-PTV). Very few researches by numerical simulation nor theoretical modeling, on the other hand, have been undertaken. Kuhlmann and Muldoon (2013) predicted the SL-2 PAS of the mode number $m = 2$ on a chaotic streamline in the bridge by employing a model flow. They noted that the four loops formed in their model were not symmetrical, which was similar to the experimental observation of the SL-2 PAS of $m = 3$ (Niigaki and Ueno 2012).

In this study, we focus on the SL-2 PAS, especially on the conditions under which it occurs, the formation time, and the surface temperature variation to distinguish their unique structure comparing to those of SL-1 PAS. Moreover, we evaluate the time required for the distributed particles to accumulate on the PAS by using a modified 'accumulation

measure' $K(t)$, that was originally proposed by Kuhlmann and Muldoon (2012). Further, we compare our results with those for the SL-1 PAS by Gotoda et al. (2015), which were obtained by the same criterion. Additionally, we analyzed the surface temperature of the liquid bridge by using an infrared (IR) camera to indicate the spatial correlation between the surface temperature distribution due to the hydrothermal wave and the SL-1 and SL-2 PASs.

Experiment

Figure 3 shows the experimental apparatus. This is almost the same as that used by Gotoda et al. (2015). The upper rod is made of sapphire that has a high thermal conductivity and that allows us to observe the liquid bridge through the rod. The bottom rod is made of aluminum, whose edge is sharpened and side wall is chemically coated in order to prevent leakage of the fluid. In the present system, we prepare a bottom rod with a tiny channel at the center, to which a tube and syringe pump are connected. This setup allows us to inject the test fluid though the bottom rod. The temperature of the bottom rod T_C is held at 20 °C by a cooling channel. The upper rod is heated by thin electric wire that is connected to a temperature controller with full closed loop proportional-integral-derivative (PID) control in order to maintain designated T_H. The flow field is visualized by adding gold-coated acrylic particles as tracers, and

Fig. 3 Experimental apparatus

1. Liquid bridge
2. Heated disk
3. Cooled disk
4. Thermocouples for T_H
5. Thermocouples for T_C
6. Heater
7. Cooling channel
8. Syringe pump tube
9. Shield
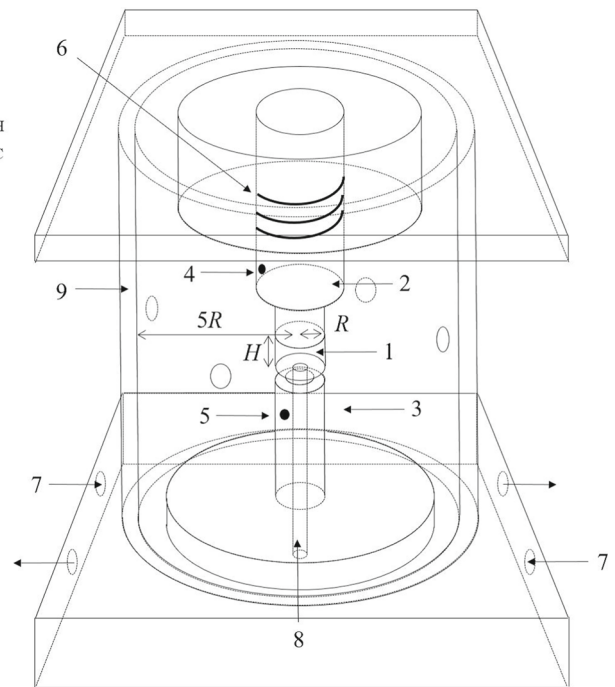
is recorded from above through the top rod and from the sides by two CCD cameras simultaneously. The whole liquid bridge is illuminated by cold light sources. Thus the detected images through the top rod indicate the projected images in the whole liquid bridge; it is impossible to distinguish the position in height of each particle with this setup. The frame rate of the CCD cameras is of 60 Hz and the exposure time is kept constant at 1/125 s. We install a coaxial external shield around the liquid bridge in order to align the thermal boundary conditions in the same way as in previous studies. The shield is provided with some small holes through which we introduce particles into the liquid bridge. We use the IR camera with a sampling rate of 500 Hz to measure the surface temperature of the liquid bridge. In this case, the shield is not installed.

The radius of the rod, R, is of 2.5 mm. The aspect ratio, $\Gamma = H/R$, is set to 0.64, 0.66, and 0.68, where H is the height of the liquid bridge. We vary the height of the liquid bridge to change the aspect ratio. Through the experiments, we fix the volume ratio V/V_0 at unity, where V is the liquid bridge volume and V_0 the volume between the coaxial disks ($= \pi R^2 H$). Even a minute loss of test liquid by evaporation can be compensated by supplying test liquid through the bottom rod from a micro syringe which is installed in a fine syringe pump in order to keep the liquid-bridge volume constant. The volume of the liquid bridge is evaluated from the images detected by the CCD camera from the side; we detect the position of the free surface, and evaluate the volume of the liquid bridge by accumulating thin cylindrical 'disks' of one pixel in height. The test fluid is 2-cSt silicone

oil, whose Prandtl number is of 28.6 at room temperature. The properties of the test fluid are listed in Table 1. We employ particles of different sizes; particle diameter d_p is of 5, 10, 15, and 30 μm, whose density ratio ρ_p/ρ_f is of 3.4, 2.5, 2.0, and 1.7, respectively, where ρ_p indicates the density of the particle and ρ_f the density of the test fluid. Density ratio has a scatter of $\pm$ 0.34. The Stokes number, St defined as follows, ranges between 1.62×10^{-6} and 29.6×10^{-6}

$$\mathrm{St} = \frac{\rho_p d_p^2}{18 \rho_f H^2}$$

We employ the 'accumulation measure' $K(t)$ originally proposed by Kuhlmann and Muldoon (2012) to quantitatively evaluate the process whereby the PAS is formed. We follow Gotoda et al. (2015) in order to evaluate $K(t)$ from the images detected through the top rod. That is, we divide the rectangle region covering the periphery of the heated disk into 50×50 cells of the same size. Each cell consists of 7×7 pixels. We then evaluate $K(t)$ defined as follows;

$$K(t) = \frac{1}{2(N_p - \overline{N})} \sum_{i=1}^{N_{\mathrm{cells}}} \left| N_i(t) - \overline{N} \right|$$

where N_p is the number of particle pixels (the white part), $\overline{N}$ is the average number of particle pixels in each cell, $N_i(t)$ is the number of particle pixels in the i-th cell at time t, and N_{cells} is the total number of cells. In our experiment, we define the number of pixels in white as the number of

Table 1 Physical properties of the test fluid (2-cSt silicone oil) at 25°C

| $\rho[kg/m^3]$	$\nu[m^2/s]$	$\kappa[m^2/s]$	$\sigma[N/m]$	$\sigma_T[N/(m\cdot K)]$
8.7×10^2	2.0×10^{-6}	7.12×10^{-8}	18.3×10^{-3}	-7×10^{-5}

particles that can be obtained from the image captured from above. It should be noted that, different from numerical simulation, N_p is not constant within the measuring period because the particles are counted in the projected image as aforementioned; there exist some particles invisible due to the overlapping and the sedimentation of the particles in the liquid bridge. By observing the process whereby SL-2 PAS is formed, we are able to quantitatively evaluate when the PAS would be formed again from the dispersal of the particles in the liquid bridge. We disperse the particles by disturbing the flow field in the liquid bridge with a thin wire inserted through the free surface. We define $t = 0$ as the instant when the wire is removed from the liquid bridge. It is noted that the flow rarely exhibits a standing-wave oscillation comparing to a traveling-wave oscillation right after the removal of the disturbing wire. We adapt the results only in the case of traveling-wave oscillation emerges in the bridge.

Results & Discussion

Figure 4 shows axial views of the accumulation patterns obtained by averaging over 500 frames with a rotating frame of reference with the fundamental frequency of the hydrothermal wave for each Marangoni number under $\Gamma = 0.68$ and $d_p = 15\ \mu$m. Noted that integrated time corresponds to $12/f_0$ for each case, where f_0 is the fundamental frequency of the hydrothermal wave. Each image shows the PAS and toroidal core as introduced by Tanaka et al. (2006) clearly. The net flow direction of the particles on the PAS is clockwise for each case, so that the rotating direction of the hydrothermal is counter-clockwise. Frames (a) and (c) indicate the SL-1 PAS and SL-2 PAS, respectively, and frame (b) the combination of the SL-1 and SL-2 PASs. In the case of SL-1 PAS (frame (a)), one can detect the toroidal core accompanying the SL-1 PAS as introduced by Tanaka et al. (2006). One can also detect another structure of the particles winding around the core (as shown as (*) in frame (a)). The PAS, toroidal core and the winding particles' structure exhibit quite similar structures of Kolmogorov-Arnold-Moser (KAM) tori, T_3^3, T_{core} and T_3^9, respectively, as predicted by Mukin and Kuhlmann (2013). These relevant structures were also indicated by Kuhlmann et al. (2014). In the case of SL-2 PAS (frame (c)), we successfully observe the same structure as Tanaka et al. (2006) firstly indicated; the PAS consists of the three major blades in the azimuthal direction, and additional looped structure emerges near the tip of each blade. One can hardly find particles forming the toroidal core nor the winding structure around the toroidal core as seen in the case of SL-1 PAS. It should be noted that there exist a larger number of particles sedimented on the bottom surface than the case of SL-1 PAS. Between the fully developed SL-1 PAS and SL-2 PAS, one can detect the combination of those structures (frame (b)), which was firstly indicated by Tanaka et al. (2006).

Fig. 4 Axial views of accumulation patterns obtained by averaging over 500 frames with the fundamental frequency of the hydrothermal wave when $\Gamma = 0.68$ and the particle size $d_p = 15\ \mu$m, for (**a**) SL-1 PAS at Ma $= 5.0\times10^4$ (the exposure time Δt is about 10 s, and the fundamental frequency $f_0 = 1.43$ Hz), (**b**) combination of SL-1 & 2 PASs at Ma $= 5.4\times10^4$ ($\Delta t \sim 12$ s, $f_0 = 1.46$ Hz) and (**c**) SL-2 PAS at Ma $= 5.8\times10^4$ ($\Delta t \sim 11$ s, $f_0 = 1.38$ Hz), (d) no PAS at Ma $= 6.4\times10^4$
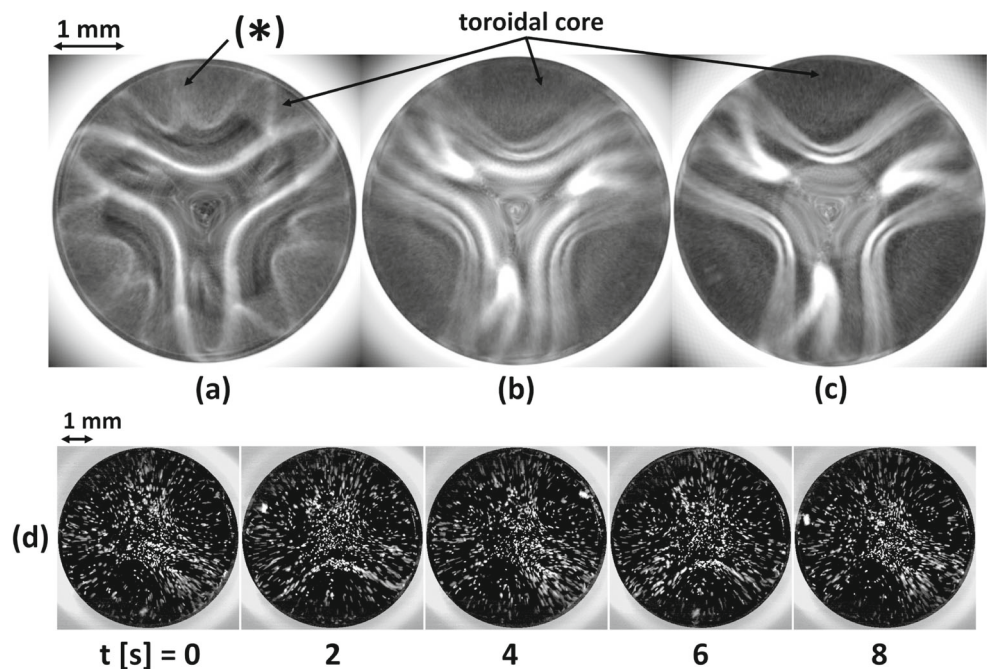
Two different structures coexist with the same frequency for traveling in the azimuthal direction. Beyond the SL-2 PAS by further increasing Ma, no more distinguishable structures like PAS are formed inside the liquid bridge; the particles disperse and rarely form ordered structures. Frame (d) in this figure shows successive images concerning 'no PAS' in the absolute frame detected through the top rod. Under such conditions, few particles occasionally accumulate on a part of PAS but do not form the fully-developed PAS even after long-enough waiting time. Even changing the particles' size considering in the present study, no PAS or ordered structures emerge in the liquid bridge. The particles' behavior seems rather chaotic as discussed by Ueno et al. (2003) and Matsugase et al. (2015). If one increases the temperature difference between the rods or the Marangoni number, the hydrothermal wave with an ordered structure collapses and no periodic flow field is observed inside the liquid bridge. Thus there exist no more KAM tori to attract the particles, resulting in the situation with almost no PAS as shown in Fig. 4(d). The temperature distribution over the free surface in this case as well as the cases with clear PASs will be illustrated later with Fig. 10.

Figure 5 illustrates the conditions under which the distinguishable PAS is formed for a particle diameter of 15 μm. Rectangular mark indicates the occurrence of SL-1 PAS, double circle indicates the SL-2 PAS, and triangle the combination of SL-1 and SL-2 PASs. Cross mark indicates the condition under which the PAS does not arise as indicated in Fig. 4(d) as an example. This graph indicates the aspect ratio $\Gamma = 0.64$ is the optimum condition under which the SL-1 PAS fully emerges. Additionally, as the aspect ratio is larger, the existence condition shifts to the region with lower Ma. Under $\Gamma = 0.66$, after SL-1 PAS occurs, the combination of SL-1 and SL-2 PASs occurs. It is found that the aspect ratio $\Gamma = 0.68$ is the optimum condition under which the SL-2 PAS fully emerges. Comparing to Tanaka
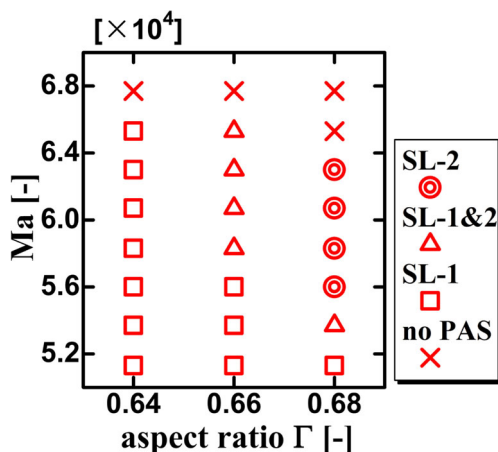

Fig. 5 Map of the particle behaviors in Ma (Marangoni number) - Γ (aspect ratio) diagram in the case of particle size $d_\mathrm{p} = 15\ \mu$m

et al. (2006), the SL-2 PAS appears in a narrower range of conditions in terms of Ma. This might be due to the larger temperature difference under the ambient air temperature of 20 °C, which leads more evaporation of the silicone oil than the experiments conducted in the refrigerator (Tanaka et al. 2006). Furthermore, another difference is the temperature of the cold rod. It has been known that the flow field and its transition point from two-dimensional steady flow to three-dimensional oscillatory flow are significantly affected by heat transfer between the liquid bridge and the ambient gas (Kamotani et al. 2003; Wang et al. 2007; Ueno et al. 2010; Yano et al. 2016). The heat transfer between the liquid bridge and the ambient gas does depend on the temperature of the cold rod because the characteristic temperature of the liquid bridge varies as the cold-rod temperature. Thus the flow field varies under the identical Marangoni number (temperature difference) as long as we change the temperature of the cold rod. The dependence of the either cold-rod temperature or ambient gas temperature on the SL-2 PAS formation, however, is not discussed because the topic of this paper would be scattered.

Figures 6 and 7 show typical examples of $K(t)$ and the subsequent images that show the process whereby the PAS forms under Ma $= 5.8 \times 10^4$, respectively. Frames (a) to (d) indicate the results with the particles of (a) 5 μm, (b) 10 μm, (c) 15 μm and (d) 30 μm in diameter, respectively. The non-dimensional time $t*$ is defined as the dimensional time t over the thermal diffusion time τ ($= H^2/\kappa$) as introduced by Gotoda et al. (2015). Under the current condition the thermal diffusion time τ is of 40.6 s. At first, we focus on the results for (b) and (c) under which the PAS clearly emerges. The value of $K(t)$ converges as time elapses, in the same way as in the simulation performed by Kuhlmann and Muldoon (2012) and as in the experiment by Gotoda et al. (2015). By comparing the series of images, as the value of $K(t)$ increases as the particles accumulate to form the PAS. It is detected that the PAS apparently forms relatively earlier ($t*\sim$0.2) in the liquid bridge than in the case of SL-1 PAS indicated by Gotoda et al. (2015). That is, more particles are forming the PAS comparing to the case of SL-1 PAS. At this stage, there exist particles not on the PAS in the liquid bridge. As time elapses, the particles gradually gather along the PAS and also travel in the toroidal core, and the fully developed state is realized at around $t* \sim 1.0$. After $t* \sim$1.0, the value of $K(t)$ converges, and the image captured through the top rod shows almost the same pattern as which the SL-2 PAS is fully formed. For (a) and (d), on the other hand, the values of $K(t)$ do not converge. In the series of images obtained with a particle size (d) $d_\mathrm{p} = 30\ \mu$m, the particles are scattered in the liquid bridge and do not accumulate on the PAS. Such situation was reproduced by the simulation (Kuhlmann and Muldoon 2012). These results indicate that the conditions under which the SL-2 PAS occurs also

Fig. 6 Typical examples of the temporal variation of $K(t)$ in the formation process of SL-2 PAS when Ma $= 5.8{\times}10^4$ in the case of (**a**) $d_\mathrm{p} = 5$ μm, (**b**) $d_\mathrm{p} = 10$ μm, (**c**) $d_\mathrm{p} = 15$ μm, and (**d**) $d_\mathrm{p} = 30$ μm. Note that the time $t*$ is indicated in thermal unit ($t* = t/(H^2/\kappa)$)
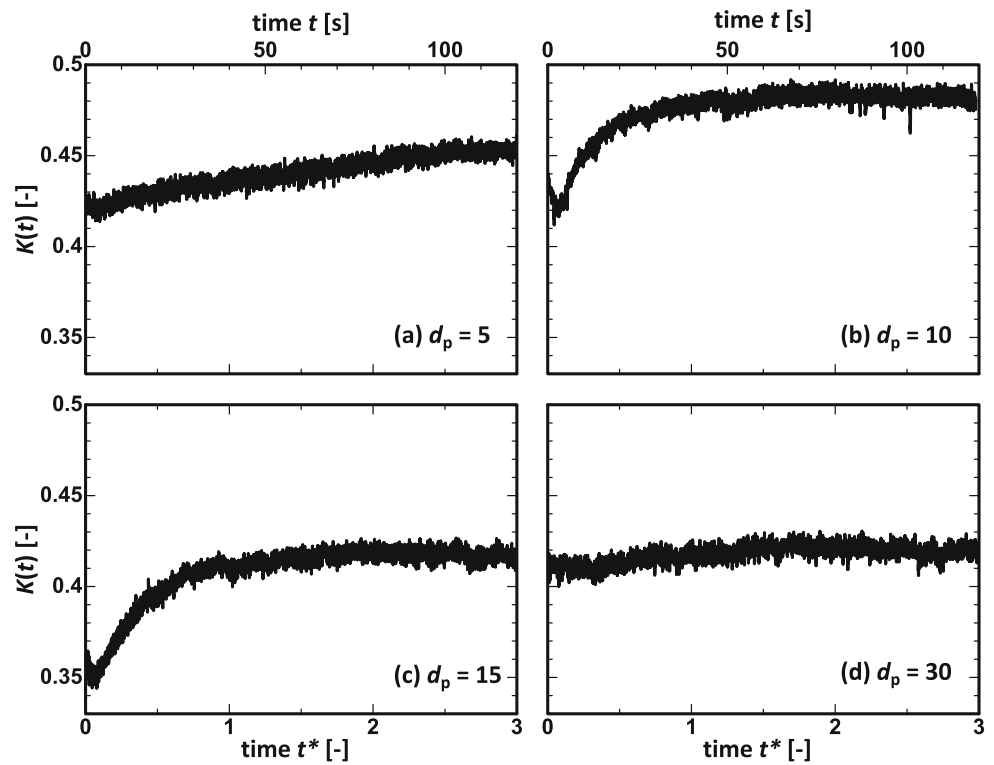
change by changing the particle size. It is noted that, under the condition of $\Delta T = 48$ K and $d_\mathrm{p} = 30$ μm, the particles are not able to accumulate to form the PAS. This can be explained by considering there are no KAM tori formed in the liquid bridge. A few particles accumulate occasionally in the liquid bridge that seems a part of the PAS. In the case

Fig. 7 Successive images of the reformation process of SL-2 PAS after the disturbance under $\Gamma = 0.68$ and Ma $= 5.8{\times}10^4$ with particles of (**a**) $d_\mathrm{p} = 5$ μm, (**b**) $d_\mathrm{p} = 10$ μm, (**c**) $d_\mathrm{p} = 15$ μm, and (**d**) $d_\mathrm{p} = 30$ μm
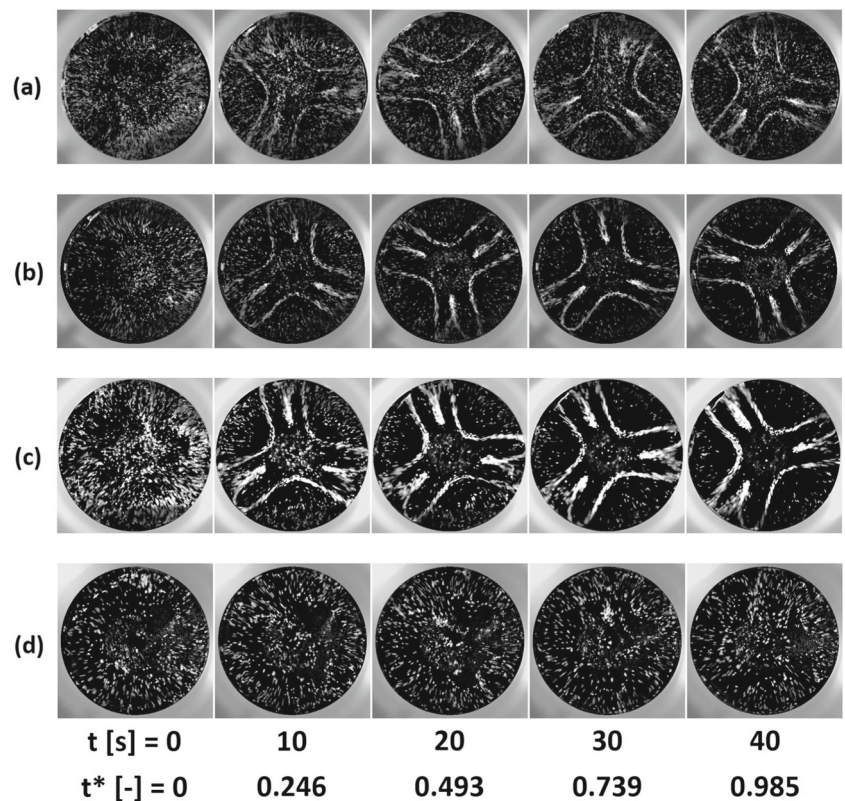
of (a) the particles of 5 μm in diameter, we surely have the SL-2 PAS, and, at the same time, we find many particles in the liquid bridge not on the PAS. We would have a variation of $K(t)$ under the current evaluation process if there exist particles not on the PAS, whose distribution would change as time elapses even after the PAS is apparently formed. Therefore, the value of $K(t)$ keeps increasing and dose not saturate in the range of 0 <t*< 3. This is a result of the particles whose density is much heavier than that of the fluid ($\rho_p/\rho_f = 3.4$). Note that we conduct a series of experiments under normal gravity condition, thus we cannot avoid the sedimentation of the particles especially in the case of larger ρ_p/ρ_f. We could not prepare spherical particles of the same size but of the different density, so that we could not discuss this effect. Further researches would be needed in order to clearly indicate the effect of St on the PAS formation.

Figure 8 indicates the formation time of the SL-2 PAS with particles of $d_p = 15$ μm (red) and of $d_p = 10$ μm (blue). We define the formation time t^*_{pas} as the instant when the value of $K(t) - K(0)$ reaches 90% of its converged value for each run. We have two main reasons for employing this definition in this manuscript; (i) in order to make a direct comparison with Gotoda et al. (2015) in which the formation time of SL-1 PAS was discussed with the same criterion, and (ii) in order to confirm ourselves to detect the final shape of the PAS and particles' distribution under each condition. In the preliminary analyses, we have tried a range of threshold to define the formation time. Note that it is sometimes quite hard to distinguish the PAS fully formed under the criterion of 50% of the converged value of $K(t) - K(0)$ as proposed by Kuhlmann et al. (2014) in the present system. This might be due to not only the sedimentation but also migration of the particles from the trajectory
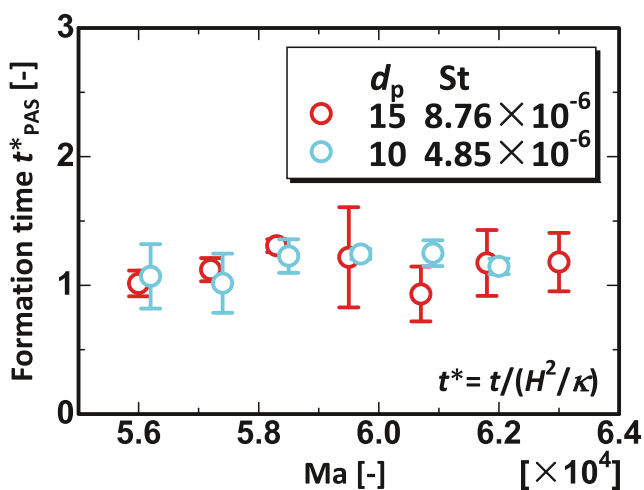
to form the PAS to the rest area of the liquid bridge because of the large density ratio. Each plot indicates an average of about five data, while the bar indicates the maximum and minimum values of the data. The data point of $d_p = 10$ μm for each Ma is intentionally shifted to distinguish each of these. It is noted that, under Ma $= 6.3 \times 10^4$ and $d_p = 10$ μm, the particles never gather along a coherent structure as the time elapses, and the SL-2 PAS does not form at all. Their data therefore is not plotted in the figure. These results indicate that the formation time of the SL-2 PAS is constant at almost unity of thermal diffusion time in spite of the variation in the temperature difference or Ma, which surprisingly coincides with the result for the SL-1 PAS (Gotoda et al. 2015). It is noted that the hydrothermal wave observed through the surface temperature measurement recovers within a period of $t^* \ll 1$ after the process of destroying the PAS. That is, the recovering process of the flow itself seems taking place much faster than the PAS reformation.

Figure 9 indicates (1) the time series of the surface temperature under fully developed states of PAS in terms of $K(t)$ (or, at $t^* > t^*_{pas}$), and (2) its power spectral density of (a) the SL-1 PAS at Ma $= 4.7 \times 10^4$ and of (b) the SL-2 PAS at Ma $= 5.8 \times 10^4$ obtained via the IR camera. In the figure a typical example of (c) the flow state at higher Ma without any stable PAS at Ma $= 6.4 \times 10^4$ is also indicated. The all data were taken from the liquid bridge of $\Gamma = 0.68$. The temperature is measured at the mid height of the liquid bridge for all cases. We select these two conditions as (a) and (b) because the most perfectly formed PASs are realized. In both cases, the surface temperature exhibits a periodic variation with a fundamental frequency and its harmonics. It is emphasized here that these temporal variations in the present study are detected by the IR camera, so that the data does not involve any other information; in case the surface temperature be measured with thermocouple (e.g., Ueno et al. 2003), the detected temperature signal does include not only the temperature variation over the free surface, but also the temperature variation in the ambient gas. This is because the relative position of the tip of the thermocouple to the free surface is periodically changed due to the dynamic surface deformation by the oscillatory flow field. In case that the surface temperature is detected by the IR camera, on the other hand, the information of the surface temperature itself is purely accumulated. By making a comparison between the cases of (a) SL-1 and (b) SL-2 PASs, the temperature variation exhibits sharper peak near the hottest point in the case of the SL-2 PAS than the case of SL-1 PAS. One notices, however, that the surface temperature variations at mid-height of the liquid bridge are quite similar in both cases. Sharper variation of the temperature in the case of SL-2 PAS results in more harmonic components in the spectrum as shown in row (2). It is noted that
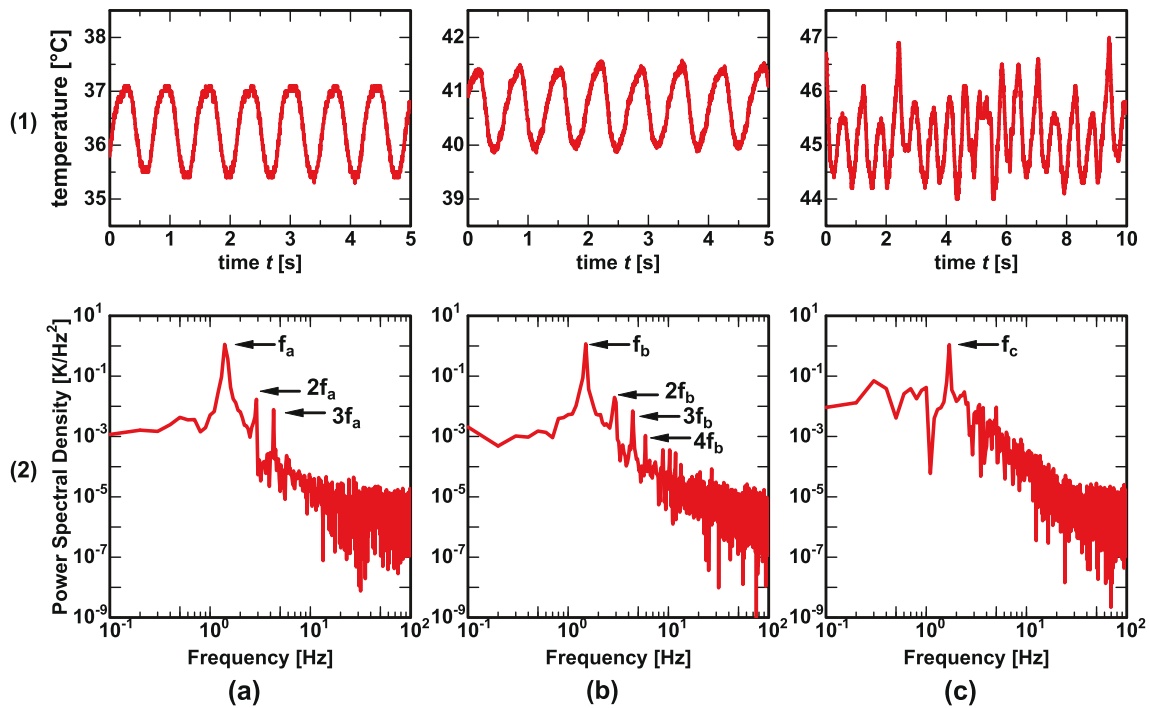

Fig. 8 Formation time of SL-2 PAS against Marangoni number for $d_p = 15$ μm (red) and $d_p = 10$ μm (blue) at $\Gamma = 0.68$. The plots indicate the averages out of five experimental runs and the bars indicate the maximum and minimum values

Fig. 9 (1) Time series of surface temperature measured at the mid height of the liquid bridge, and (2) its power spectral density for (**a**) SL-1 PAS at Ma $= 4.7 \times 10^4$, (**b**) SL-2 PAS at Ma $= 5.8 \times 10^4$, and (**c**) no stable PAS at Ma $= 6.4 \times 10^4$

such a spectrum with a fundamental frequency and its higher harmonics can be seen in the oscillatory flows in the liquid bridge without any PASs under normal gravity (Ueno et al. 2003) and also microgravity (Sato et al. 2013; Matsugase et al. 2015) before the flow exhibits chaotic behaviors. Once the particles disperse, and no distinct structures are formed in the liquid bridge (as shown in (c)), the surface temperature varies vigorously, and the peaks in frequency are buried in the spectrum except the fundamental frequency. In the following, we focus on the whole temperature field over the free surface to discuss the differences between the SL-1 and SL-2 PASs.

Figure 10 shows the spatio-temporal diagrams (STD) for (a) SL-1 PAS at Ma $= 4.7 \times 10^4$, (b) SL-2 PAS at Ma $= 5.8 \times 10^4$, and (c) almost no PAS at Ma $= 6.4 \times 10^4$ in the case of $\Gamma = 0.68$. These conditions correspond to those shown in Fig. 9. The STD illustrates the distribution of the deviation of the surface temperature from the averaged temperature detected by the IR camera as a function of time at each height along the center line of the liquid bridge in the axial direction. It is noted that we measure the surface temperature by the IR camera with narrower range of the temperature than the temperature difference between the rods sustaining the liquid bridge in order to resolve a small amount of temperature deviation. That is, in the case of (a) SL-1 PAS, the temperatures of heated and cooled disks are of 60 °C (T_H) and 20 °C (T_C), respectively. The measuring range of the IR camera, $T_{\min} \le T \le T_{\max}$, in that case

is from 25 to 42 °C, in order to avoid measuring a significant change of the temperature in the thermal boundary layers near the end rods. The measuring range of the IR camera as well as the end-rod temperatures for (b) and (c) is indicated in the figure caption. The surface temperature variations (top) are illustrated in non-dimensional manner as $(T - T_{\min})/(T_{\max} - T_{\min})$, so that the temperature distribution near the hot-end and cold-end rods does not illustrate the temperature in a range between T_H and $T_{\max}$ and between $T_{\min}$ and T_C, respectively. The temperature deviation (bottom) is also illustrated in non-dimensional manner; the temperature deviation is divided by its maximum value. Apparently, both STDs in the cases of two kinds of PAS ((a) SL-1 PAS and (b) SL-2 PAS) exhibit similar structures. That is, periodic variation of the surface temperature is realized all over the surface, and the 'thermal wave' reflecting the hydrothermal wave propagates from the colder-end surface to the hotter-end surface. This is a typical behavior of the hydrothermal wave in the short (or low aspect-ratio) liquid bridge of high Pr fluids (e.g., Muehlner et al. 1997). In the case of longer (or higher aspect-ratio) liquid bridge, the traveling direction seems opposite (Sato et al. 2013; Ueno et al. 2014). Once (c) the PAS breaks apart and no ordered structures are formed by increasing Ma (as also shown in Fig. 4(d)), the surface temperature never exhibits a periodic STD as seen under the conditions of SL-1 and SL-2 PASs. Any periodic flow structures are not formed inside the liquid bridge, and the particles never accumulate to realize the PAS.
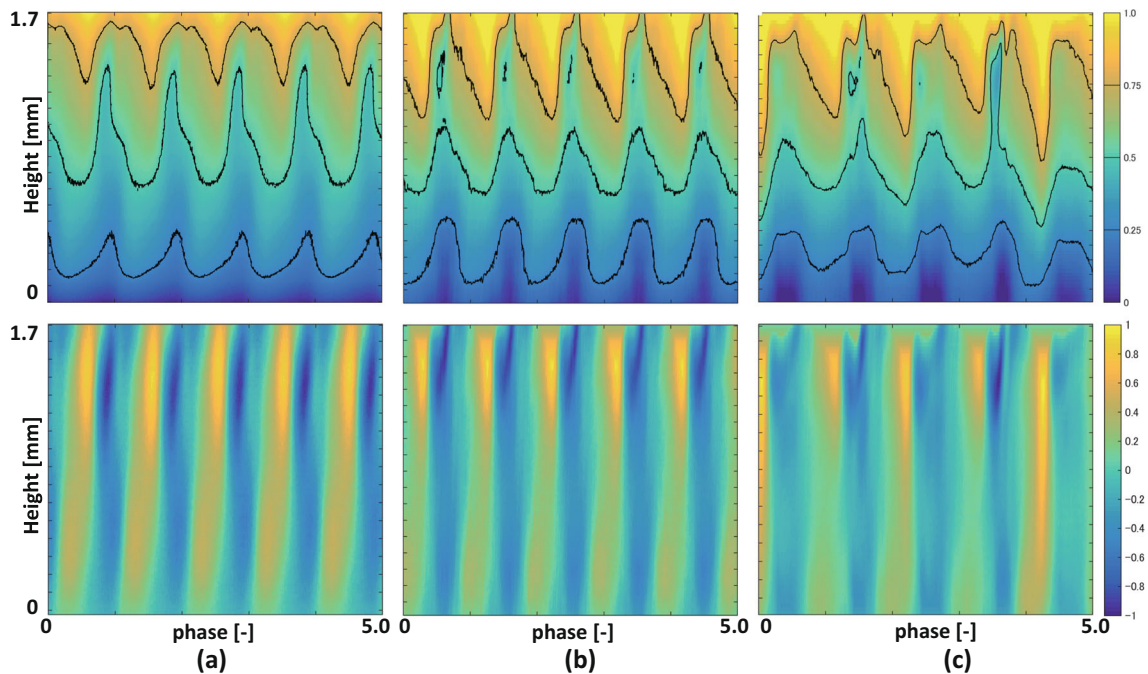
Fig. 10 Spatio-temporal diagram of surface temperature (top) and temperature deviation (bottom) of liquid bridge (**a**) SL-1 PAS at Ma $= 4.7 \times 10^4$ ($T_H = 60$ °C and $T_C = 20$ °C), (**b**) SL-2 PAS at Ma $= 5.8 \times 10^4$ ($T_H = 68$ °C, $T_C = 20$ °C), and (**c**) no stable PAS at Ma $= 6.4 \times 10^4$ ($T_H = 76$ °C, $T_C = 20$ °C). Note that the temperature range measured by the IR camera [T_{min}, T_{max}] is intentionally narrower than the temperature difference, that is, $T_C < T_{min}$ $\leq T \leq T_{max} < T_H$. The temperature range measured by the IR camera for each case is as follows; (**a**) $T_{max} = 42$ °C and $T_{min} = 25$ °C, (**b**) $T_{max} = 45$ °C and $T_{min} = 30$ °C, and (**c**) $T_{max} = 50$ °C and $T_{min} = 40$ °C. The absolute temperature variations and their deviations (bottom) are illustrated in non-dimensional manner as $(T-T_{min})/(T_{max}-T_{min})$ and T'/T'_{max}, respectively

Figure 11 illustrates (1) the top views of the PASs, (2) and (3) the absolute temperature and the temperature deviation over the free surface in a range of $0 \leq \theta \leq 2\pi/3$ as defined in (1), respectively, for (a) SL-1 PAS (Ma $= 4.7 \times 10^4$) and (b) SL-2 PAS (Ma $= 5.8 \times 10^4$). The distributions of the surface temperature and its deviation are reconstructed from the data shown in Fig. 10 by considering propagation speed in azimuthal direction of the HW as conducted by Sato et al. (2013) and Ueno et al. (2014). Frames (2) and (3) are redrawn from the same data shown in Figs. 10(a) and (b). In that figure, the position 1 indicates the azimuthal position where the particles on the PAS approach very close to the free surface (close to 'collision point' defined by Hofmann and Kuhlmann (2011)), and position 2 indicates the azimuthal position where the particles on the PAS 'detach' from the free surface and go back to the bulk of the liquid bridge (closed to 'release point'). Note that we did not track the particles in three dimensional system, so that we could not surely insist whether the particles absolutely 'detach' from the free surface. In the case of (a) SL-1 PAS, the particles on the PAS approach near the free surface (position 1), where the larger temperature deviation in positive variation (hottest spot, hereafter) is realized. Then the particles flow down along the free surface, and detach to penetrate inside the liquid bridge, where the temperature deviation is closed

to neutral (position 2). Such positions match quite well with the results shown by Gotoda et al. (under review) in spite of the differences of the aspect ratio and Marangoni number, but are different from the result by Schwabe et al. (2007) with a fluid of Pr ~ 16. Difference of the spatial correlation between the PAS and surface temperature deviation comes from the difference of flow field inside the liquid bridge due to the difference of Pr as indicated by Gotoda et al. (under review). In the case of SL-2 PAS, on the other hand, the particles on the PAS approach the free surface again due to the additional loop (position 1'), and then the particles 'detach' again from the free surface (position 2'). It is found that the spatial correlation between those positions (1 and 2) and the temperature deviation in the case of the SL-2 PAS almost corresponds to that in SL-1 PAS. We emphasize that the existing range of the first 'blade' of the SL-2 PAS in terms of azimuthal position almost corresponds to that of the SL-1 PAS's blade. Then the particles on the SL-2 PAS approach the free surface again due to the additional loop near the free surface (position 1'), where the temperature deviation in negative variation (coldest spot, hereafter) is realized. The particles on the SL-2 PAS then go downward along the free surface toward the relatively coldest spot in the bottom half of the liquid bridge (position 2'), and then detach again the free surface to penetrate the inside the liquid bridge. As

Fig. 11 (1) Top views of the PASs, (2) and (3) the absolute temperature and the temperature deviation over the free surface in a range of $0 \leq \theta \leq 2\pi/3$ (as defined in (1)), respectively, for (**a**) SL-1 PAS (Ma = 4.7×10^4) and (**b**) SL-2 PAS (Ma = 5.8×10^4). The distributions of the surface temperature and its deviation are reconstructed from the data shown in Fig. 10 by considering propagation speed in azimuthal direction of the HW as conducted by Sato et al. (2013) and Ueno et al. (2014). Frames (2) and (3) are redrawn from the same data shown in Fig. 10(a) and (b)
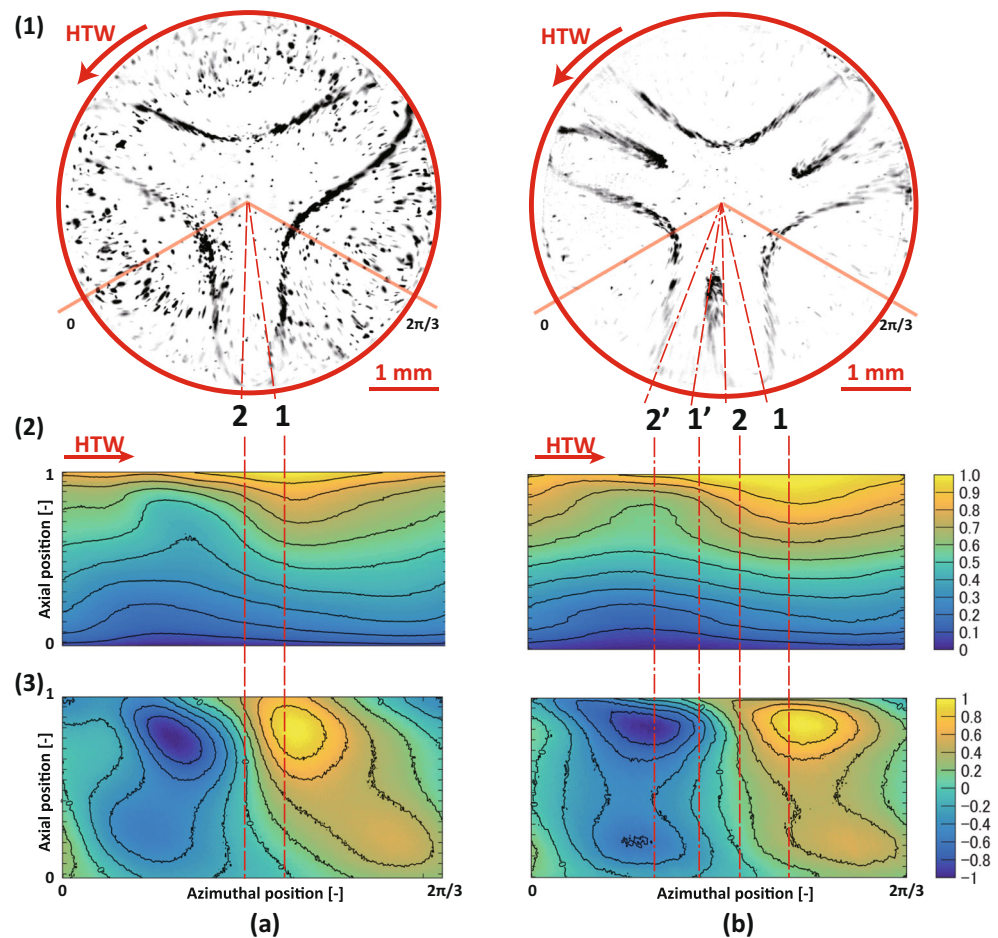
aforementioned, Gotoda et al. (under review) indicated that the particles on the PAS are not gathered by thermocapillary effect due to the temperature variation on the free surface as proposed by Schwabe et al. (2007). The spatial structure that the particles gather to form is determined by the flow structure itself in the liquid bridge. In order to resolve correlation between the particle trajectories and the thermal-flow field, direct numerical simulations with significantly fine spatio-temporal resolutions would be needed.

Conclusion

We focus on the SL-2 PAS, one of the major particles accumulation structures emerging in thermocapillary-driven convection in the half-zone liquid bridge. We realize the SL-2 PAS as well as SL-1 PAS in the bridge of high Prandtl number liquid with particles of $5 - 30 \, \mu$m in diameter, under the corresponding conditions of small Stokes number of the order of $10^{-6} \sim 10^{-5}$.

We illustrate the existing conditions of SL-1 PAS, SL-2 PAS and the combination of those against the Marangoni number and the liquid-bridge aspect ratio. Then the shape

of the SL-2 PAS in the rotating frame of reference with hydrothermal wave is described by the observation through the transparent top rod. The formation time of the PAS is evaluated by employing modified accumulation measure $K(t)$, and is found to be around unity in the thermal diffusion unit. Distributions of the surface temperature and its deviation from the averaged field are indicated to distinguish the SL-1 PAS and SL-2 PAS.

References

Abe, Y., Ueno, I., Kawamura, H.: Effect of shape of HZ liquid bridge on particle accumulation Structure (PAS). Microgravity Sci. Technol. **19**, 84–86 (2007)

Gotoda, M., Sano, T., Kaneko, T., Ueno, I.: Evaluation of existence region and formation time of particle accumulation structure (PAS) in half-zone liquid bridge. Eur. Phys. J. Special Topics **224**(2), 299–307 (2015)

Gotoda, M., Toyama, A., Ishimura, M., Sano, T., Suzuki, M., Kaneko, T., Ueno, I.: Experimental study on dynamics of finite-size particles in coherent structures induced by thermocapillary effect in deformable liquid bridge. Phys. Rev. Fluids (under review)

Hirata, A., Nishizawa, S., Sakurai, M.: Experimental results of oscillatory Marangoni convection in a liquid bridge under normal gravity. J. Jpn. Soc. Microgravity Apply **14**, 122–129 (1997)

Hofmann, E., Kuhlmann, H.C.: Particle accumulation on periodic orbits by repeated free surface collisions. Phys. Fluids **23**(7), 072106 (2011)

Kamotani, Y., Wang, L., Hatta, S., Wang, A., Yoda, S.: Free surface heat loss effect on oscillatory themocapillary flow in liquid bridges of high Prandtl number fluids. Int. J. Heat Mass Transf. **46**(17), 3211–3220 (2003)

Kuhlmann, H.C., Mukin, R.E., Sano, T., Ueno, I.: Structure and dynamics of particle-accumulation in thermocapillary liquid bridges. Fluid Dyn. Res. **46**, 041421 (2014)

Kuhlmann, H.C., Muldoon, F.H.: Particle-accumulation structures in periodic free-surface flows: inertia versus surface collisions. Phys. Rev. E **85**, 046310 (2012)

Kuhlmann, H.C., Muldoon, F.H.: On the different manifestations of particle accumulation structures (PAS) in thermocapillary flows. Eur. Phys. J. Special Topics **219**, 59–69 (2013)

Matsugase, T., Ueno, I., Nishino, K., Ohnishi, M., Sakurai, M., Matsumoto, S., Kawamura, H.: Transition to chaotic thermocapillary convection in a half zone liquid bridge. Int. J. Heat Mass Transf. **89**, 903–912 (2015)

Melnikov, D.E., Pushkin, D.O., Shevtsova, V.M.: Synchronization of finite-size particles by a traveling wave in a cylindrical flow. Phys. Fluids **25**, 092108 (2013)

Melnikov, D.E., Watanabe, T., Matsugase, T., Ueno, I., Shevtsova, V.: Experimental study on formation of particle accumulation structures by a thermocapillary flow in a deformable liquid column. Microgravity Sci. Technol. **26**, 365–374 (2014)

Muehlner, K.A., Schatz, M.F., Petrov, V., McCormick, W.D., Swift, J.B., Swinney, H.L.: Observation of helical traveling-wave convection in a liquid bridge. Phys. Fluids **9**, 1850–1852 (1997)

Mukin, R.V., Kuhlmann, H.C.: Topology of hydrothermal waves in liquid bridges and dissipative structures of transported particles. Phys. Rev. E **88**, 053016 (2013)

Muldoon, F.H., Kuhlmann, H.C.: Coherent particulate structures by boundary interaction of small particles in confined periodic flows. Phys. D: Nonlinear Phenomena **253**, 40–65 (2013)

Muldoon, F.H., Kuhlmann, H.C.: Different particle-accumulation structures arising from particle–boundary interactions in a liquid bridge. Int. J. Multiphase. Flow **59**, 145–159 (2014)

Muldoon, F.H., Kuhlmann, H.C.: Origin of particle accumulation structures in liquid bridges: Particle–boundary-interactions versus inertia. Phys. Fluids **28**, 073305 (2016)

Niigaki, Y., Ueno, I.: Formation of particle accumulation structure (PAS) in Half-Zone liquid bridge under an effect of Thermo-Fluid flow of ambient gas, transactions of the Japan soc. For aeronautical and space sci. Aerospace tech. Japan10 Ph33-Ph37 (2012)

Pushkin, D.O., Melnikov, D.E., Shevtsova, V.M.: Ordering of small particles in one-dimensional coherent structures by time-periodic flows. Phys. Rev. Lett. **106**, 234501 (2011)

Sato, F., Ueno, I., Kawamura, H., Nishino, K., Matsumoto, S., Ohnishi, M., Sakurai, M.: Hydrothermal wave instability in a high-Aspect-Ratio Liquid Bridge of Pr 200. Microgravity Sci Technol. **25.1**, 43–58 (2013)

Schwabe, D., Hintz, P., Frank, S.: New features of thermocapillary convection in floating zones revealed by tracer particle accumulation structures (PAS). Microgravity Sci. Technol. **9**, 163–183 (1996)

Schwabe, D., Mizev, A.I., Udhayasankar, M., Tanaka, S.: Formation of dynamic particle accumulation structures in oscillatory thermocapillary flow in liquid bridges. Phys. Fluids **19**(7), 072102 (2007)

Schwabe, D., Mizev, A., Tanaka, S., Kawamura, H.: Particle accumulation structures in time-dependent thermocapillary flow in a liquid bridge under microgravity. Microgravity Sci. Technol. **18**(3-4), 117–127 (2006)

Tanaka, S., Kawamura, H., Ueno, I., Schwabe, D.: Flow structure and dynamic particle accumulation in thermocapillary convection in a liquid bridge. Phys. Fluids **18**, 067103 (2006)

Ueno, I., Kawasaki, H., Watanabe, T., Motegi, K., Kaneko, T.: Hydrothermal-wave instability and resultant flow patterns induced by thermocapillary effect in a half-zone liquid bridge of high aspect ratio, 15th Int. Heat Transfer Conf. (IHTC15), paper #: IHTC15-9489 (12 pages), doi:10.1615/IHTC15.fcv.009489 (2014)

Ueno, I., Kawazoe, A., Enomoto, H.: Effect of ambient-gas forced flow on oscillatory thermocapillary convection of half-zone liquid bridge. Fluid Dynamics Materials Processing **6**, 99–108 (2010)

Ueno, I., Tanaka, S., Kawamura, H.: Oscillatory and chaotic thermocapillary convection in a half-zone liquid bridge. Phys. Fluids **15**(2), 408–416 (2003)

Wang, A., Kamotani, Y., Yoda, S.: Oscillatory thermocapillary flow in liquid bridges of high Prandtl number fluid with free surface heat gain. Int. J. Heat Mass Transf. **50**(21–22), 4195–4205 (2007)

Wanschura, M., Shevtsova, V.M., Kuhlmann, H.C., Rath, H.J.: Convective instability mechanisms in thermocapillary liquid bridges. Phys. Fluids **7**, 912–925 (1995)

Watanabe, T., Melnikov, D.E., Matsugase, T., Shevtsova, V.M., Ueno, I.: The stability of a thermocapillary-buoyant flow in a liquid bridge with heat transfer through the interface. Microgravity Sci. Technol. **26.1**, 17–28 (2014)

Yano, T., Maruyama, K., Matsunaga, T., Nishino, K.: Effect of ambient gas flow on the instability of Marangoni convection in liquid bridges of various volume ratios. Int. J. Heat Mass Transf. **99**, 182–191 (2016)